

## Integration of in-situ load experiments and numerical modeling in a long-term bridge monitoring system on a newly-constructed widened section of freeway in Taiwan

Yi-Tsung Chiu<sup>1a</sup>, Tzu-Kang Lin<sup>2b</sup>, Hsiao-Hui Hung<sup>3c</sup>, Yu-Chi Sung<sup>\*1,3</sup> and Kuo-Chun Chang<sup>3,4d</sup>

<sup>1</sup>Department of Civil Engineering, National Taipei University of Technology, 1, Zhongxiao E. Rd. Sec. 3, Taipei 106, Taiwan R.O.C.

<sup>2</sup>Department of Civil Engineering, National Chiao Tung University, 1001, University Rd., Hsinchu 300, Taiwan R.O.C.

<sup>3</sup>National Center for Research on Earthquake Engineering, 200, Hsinhai Rd. Sec. 3, Taipei 10, Taiwan R.O.C.

<sup>4</sup>Department of Civil Engineering, National Taiwan University, 1, Roosevelt Rd. Sec. 4, Taipei 106, Taiwan R.O.C.

(Received December 12, 2013, Revised April 25, 2014, Accepted April 30, 2014)

**Abstract.** The widening project on Freeway No.1 in Taiwan has a total length of roughly 14 kilometers, and includes three special bridges, namely a 216 m long-span bridge crossing the original freeway, an F-bent double decked bridge in a co-constructed section, and a steel and prestressed concrete composite bridge. This study employed in-situ monitoring in conjunction with numerical modeling to establish a real-time monitoring system for the three bridges. In order to determine the initial static and dynamic behavior of the real bridges, forced vibration experiments, in-situ static load experiments, and dynamic load experiments were first carried out on the newly-constructed bridges before they went into use. Structural models of the bridges were then established using the finite element method, and in-situ vehicle load weight, arrangement, and speed were taken into consideration when performing comparisons employing data obtained from experimental measurements. The results showed consistency between the analytical simulations and experimental data. After determining a bridge's initial state, the proposed in-situ monitoring system, which is employed in conjunction with the established finite element model, can be utilized to assess the safety of a bridge's members, providing useful reference information to bridge management agencies.

**Keywords:** bridge monitoring system; in-situ experiment; position sensitive detector

### 1. Introduction

---

\*Corresponding author, Professor, E-mail: [sungyc@ntut.edu.tw](mailto:sungyc@ntut.edu.tw)

<sup>a</sup> Ph.D. Student, E-mail: [my95340390@gmail.com](mailto:my95340390@gmail.com)

<sup>b</sup> Assistant Professor, E-mail: [tklin@nctu.edu.tw](mailto:tklin@nctu.edu.tw)

<sup>c</sup> Associate Research Fellow, E-mail: [hhung@ncrec.narl.org.tw](mailto:hhung@ncrec.narl.org.tw)

<sup>d</sup> Professor, E-mail: [kcchang@ncrec.narl.org.tw](mailto:kcchang@ncrec.narl.org.tw)

A typical bridge monitoring system comprises a sensor system, data acquisition system, data communications and transmission system, and data analysis and processing system. The establishment of a reliable and stable monitoring system requires careful attention to system selection, monitoring items, sensor installation and maintenance, and interpretation of the resulting physical quantities. In addition, specific knowledge of the original intention of the bridge design and the dynamic characteristics of the bridge structure is also required.

The real dynamic behavior of a bridge is usually determined by measuring the dynamic response at observation points when a load is moving on the bridge. In the field of civil engineering, an accelerometer or velocity meter is conventionally used to determine the displacement of specific points at different times. For instance, eleven accelerometers were installed on the West Street On-Ramp Bridge to monitor the vibration caused by traffic flow between 2002 and 2010. A total of 1,350 events, including six earthquakes, were recorded (Gomez *et al.* 2011). Analysis showed that the fundamental frequency changed due to the aging of the structure, but no damage was observed. Exploiting the advantages of fiber Bragg grating (FBG) sensors, which include easy deployment, low-loss transmission, and immunity to electromagnetic interference, Chan *et al.* (2006) mounted such sensors on Hong Kong's Tsing Ma Bridge to perform structural health monitoring. The resulting data was used to assess the response of various parts of the bridge to vehicular and train traffic. A monitoring system was further installed on the Tsing Ma Bridge in 1997 to perform comparisons and judge the health status of the bridge. Fiber-optic strain sensors were used by Costa *et al.* (2012) to perform long-term monitoring, assess bridge reliability, and obtain data needed to perform fatigue assessment. A neural network-based regression model describing the relationship between thermal effects and natural frequency of a box girder bridge was proposed by Cury *et al.* (2012) with the support of a long-term monitoring database, and slight modification of the regression model was performed after the retrofitting of the bridge. Optical fiber Bragg grating sensors embedded in glass fiber reinforced polymer (GFRP-OFBGS) was used to monitor the dynamic behavior of bridge suspenders by Li *et al.* (2012), and long-term monitoring was conducted on an in-use suspension bridge to evaluate the fatigue condition of the suspenders.

As distortion may affect displacement measurements during the processing of digital signals from conventional instruments, numerous researchers have developed optical non-contact displacement measurement methods. Because these methods can directly measure displacement without numerical integration error, application to experimental measurements has been widely considered. An optical tracking system measuring displacement of the lower level of Britain's Humber Bridge was used by Stephen *et al.* (1993). In this system, the tracking of objects was performed by selecting the objects' initial characteristics and repeatedly using the least squares method, which enabled the extremely low frequency movements of the bridge to be successfully measured. Olaszek (1999) developed a method of determining the dynamic characteristics of a bridge foundation employing photography and an extra reference system. In this method, reference points and target points were measured simultaneously, which eliminated the effect of parallel movement when imaging. The reference correction method is not applicable to rotating movements, however, and a specially-made optical element must be used to enable a single imaging device to simultaneously capture two relatively distant points (reference point and target point).

A system comprising a high-frequency camera with a resolution of 520 lines and a 450 zoom capability was deployed by Wahbeh *et al.* (2003) to track a black target consisting of a thin steel plate with a width of 28" and 32", upon which two high-resolution red LEDs were mounted. This

system was used to measure the displacement of the Vincent Thomas Bridge in California. The complex signal processing operations included simplification of optical data and use of nonlinear Gaussian regression curves to define the centers of the high-intensity red spots. The system was applied to record 30 min. of optical data for use in an offline model.

Microwave interferometers have been used in conjunction with an imaging capability to measure the deflection of truly large-scale structures. However, the equipment needed for this approach is extremely costly and difficult to use. Nassif *et al.* (2005) compared the results of dynamic live load experiments employing contact sensors with data obtained using a non-contact laser Doppler dynamic gauge system. The laser Doppler vibrometer (LDV) system functioned like a non-contact method, and the bridge vibration and deflection test results obtained using this nondestructive system proved to be more precise than measurements using an LVDT system mounted directly on the bridge. In addition, compared with the use of fixed geophone sensors, the LDV system was able to provide fast and accurate measurements. Lee *et al.* (2006) used digital photography and digital image processing technology to measure dynamic displacement. This technique is very inexpensive and easy to implement, and is still a viable alternative to high-resolution dynamic measurements. A Position Sensitive Device (PSD) was applied by Sung *et al.* (2012) to monitor the dynamic displacement of a bridge deck caused by truck loading, and demonstrated that measurement resolution can be effectively improved.

Accompanying the development of sensing technologies, researchers have also studied use of numerical modeling in damage detection. To investigate the relationship between existing and newly-grouted concrete in the Versoix bridge, Inaudi *et al.* (1999) performed theoretical study of low-coherence fiber optical sensors, and used the sensors to perform long-term monitoring of concrete displacement, which allowed the detection of developing concrete cracks. The deformation of the bridge was then derived employing the double integral of the horizontal and vertical curvatures measured locally. A method of measuring bridge deflection employing fiber optic grating sensors was developed by Kim and Cho *et al.* (2004). This method relied on measurement of the strain at several points to continuously recalculate longitudinal deflection employing a formula based on conventional beam theory. A strain function was derived from the measured strain data using regression analysis, and a deflection curve was obtained using a strain function formula. This method has some restrictions, however. The dependent variable is highly vulnerable to perturbations, which implies that measurements at many points are needed to accurately estimate a bridge's deflection. Patjawit *et al.* (2005) used the tap test to obtain bridges' flexibility matrices, and employed these to establish global flexibility indexes, which provide a basis for judging the degree of damage to a bridge. Ribeiro *et al.* (2012) measured the ambient vibration of a bowstring-arch railway bridge employing accelerometers, and developed a finite element model to perform comparisons. To improve consistency of the numerical model, the Genetic Algorithm (GA) was also applied in parameter optimization. Since only the static and dynamic response of a bridge at observation points can be obtained by monitoring after a bridge has been completed and is in service, and the degrees to which specific bridge members are affected by external forces cannot be obtained, it is necessary to rely on numerical modeling to make up for this deficiency. However, the reliability of numerical modeling must be checked through in-situ experiments before it can be used in conjunction with monitoring data to perform clear and reliable assessment of bridge health. As a result, the finite element method is applied in this study in conjunction with experimental data to construct a model that can be used in a comprehensive bridge monitoring system. As the finite element model must express a bridge's real characteristics before it can be successfully validated, a series of experiments, including forced

vibration experiment, static load experiment, and dynamic load experiment, was conducted as follows:

While ambient vibration measurements can be used to determine the natural vibration frequency and period of a real bridge, accuracy may be poor if the amplitude of free vibration measurements is too small. Forced vibration can therefore be used to analyze the dynamic behavior of a bridge. The application of a specific vibration frequency to a bridge can then be employed to collect vibration signals from the bridge structure. If the natural frequency of the bridge is close to the imposed frequency, the amplitude of the signal will increase significantly as a consequence of resonance caused by the bridge's structural dynamics, and when measured in-situ, a significant increase in amplitude can readily be sensed.

Following the forced vibration test, the stiffness and dynamic deformation of a bridge should also be evaluated. The most direct way to obtain the load deformation of a real bridge is to apply a static load to the bridge, and measure the displacement of structural observation points by installing on the underside conventional displacement sensors, such as linear variable differential transformers (LVDTs). As the use of wire-connected equipment may possibly be detrimental to accuracy, this paper proposes the use of a laser rangefinder and level measurements to determine static deformation, as well as the employment of position sensitive devices (PSDs). The dynamic response of bridges, which can effectively eliminate error from numerical integration through the use of more precise dynamic displacement data, can be obtained directly via this approach.

The remainder of this paper is organized as follows: First, the structure of the proposed bridge monitoring system, the mechanical characteristic of the three special bridges, and the corresponding long-term monitoring sensors are introduced in section 2. The in-situ experiments, including the forced vibration test, static load test, and the dynamic test, are carried out utilizing conventional instrumentation and PSDs. In order to realize a long-term monitoring system, models for three special bridges based on the finite element method (FEM) are constructed and compared with the experimental data in section 4. Finally, a summary is provided, and conclusions are drawn.

## **2. The proposed bridge monitoring system**

The bridge monitoring system employed in this study involves the integration of the finite element model established from in-situ experimental data, obtained via forced vibration experiments, static load experiments, and dynamic load experiments, and long-term monitoring (see Fig. 1). Based on the database compiled from the results of long-term monitoring, the state of damage at a specific location can be numerically simulated with the support of the fine-tuned finite element model, and an alarm threshold can be set in advance. Rapid diagnosis and evaluation can then be conducted to provide reference information to bridge managers when anomalies are observed during monitoring.

Different types of sensor were deployed in in-situ bridge experiments and long-term bridge monitoring systems in order to understand the short-term and long-term behavior of the monitored bridges. The deployment of sensors in the in-situ bridge experiments sought to capture the actual behavior of the three bridges, and sensors were located on the critical sections with the maximum physical quantities in the long-term bridge monitoring system. The specific arrangement of the sensors enabled determination of the mechanical characteristics of static, dynamic and long-term loads, including those caused by temperature changes and earthquakes. In view of the data types

and sampling frequency, the long-term monitoring framework used different data acquisition systems, including as those employing static and dynamic data acquisition. The data acquired from these systems was ultimately incorporated in a single database for use in analysis and decision-making. In addition, an in-situ experiment was performed on a newly-completed bridge that had not yet entered use in order to acquire the bridge's static and dynamic characteristics. This data was applied to improve the numerical model created using the finite element method, which completed the bridge monitoring system as a whole.

By utilizing the proposed monitoring system, data concerning the structural behavior and abnormalities of similar bridge types can be established. Apart from immediate use to shed light on bridge usage and structural safety, the collected data can also be used as a reference for the future design of bridges of the same type, and can guide bridge maintenance. The system can detect structural behavioral abnormalities or deterioration at an early date, allowing the adoption of remedial measures ahead of time. This will diminish uncertainty concerning structural safety, reduce long-term management costs and risk, and ultimately extend bridge life. Moreover, through the support of the established finite element model, the deployed sensors in the proposed system can be used to monitor the real-time condition of the three bridges with only a limited maintenance budget. Based on the monitoring results, additional sensors can be considered on sections possibly suffering damage, strengthening the performance of the system.

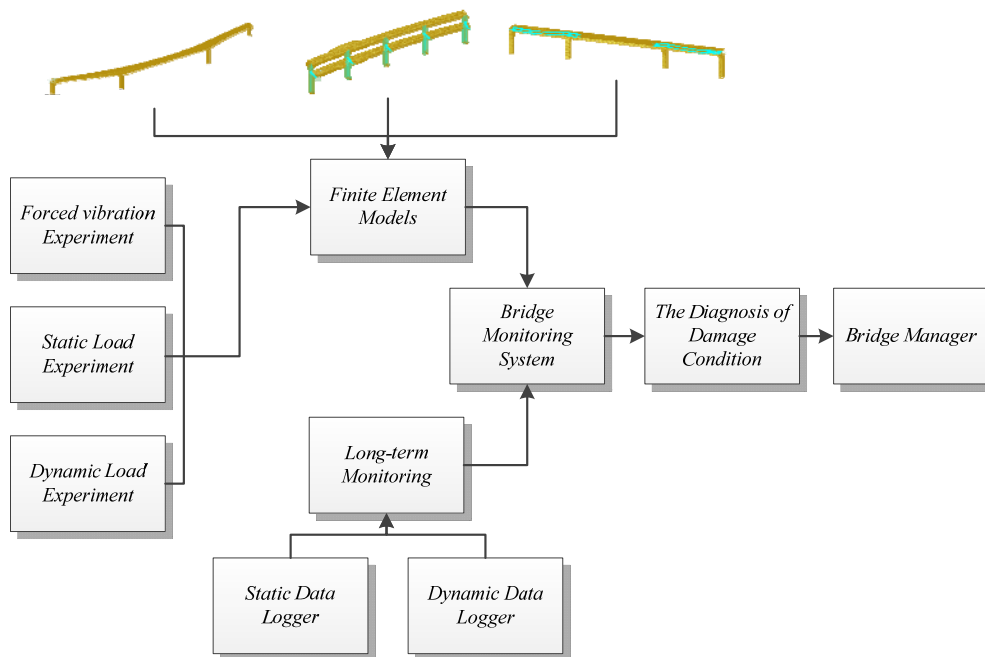


Fig. 1 Bridge Monitoring System

The three special bridges subjected to long-term monitoring in this study consisted of a long-span bridge crossing the original freeway system, an F-bent double decked bridge in the co-constructed section, and a steel and prestressed concrete composite bridge. All of these bridges were equipped with thermometers, vibrating wire strain gauges, Linear Variable Differential Transformers (LVDTs), strong-motion accelerometers, and inclinometers, including both conventional and micro electro mechanical systems (MEMS) systems. These sensors were used in the monitoring system due to their high stability and reliability. The dynamic data logger was triggered automatically when the measured peak ground acceleration (PGA) exceeded a threshold of 10 gal, and the static data logger recorded data continuously with at a constant interval of 10 minutes. The following is a brief description of the three special bridges:

#### Long-span Bridge

In order to avoid a geological sensitive area, the northbound lanes of Freeway No.1 must cross three spans (135 m, 216 m, and 135 m), on four piers numbered P353 and P4A01 through P4A03. The main span of this freeway-crossing bridge is currently the steel box girder bridge with the longest span (216 m) in Taiwan, and is the most distinctive engineering feature in this highway section (Fig. 2). Because the center of the main span is subject to vibration from earthquakes and traffic, it is highly vulnerable to deformation, and the great length of the bridge as a whole indicates that the bridge may experience uneven temperature distribution in the direction of traffic. Furthermore, because of the large beam depth, a temperature gradient often exists along the beam depth direction, and has caused unforeseen deflection curvature. In addition, since the bridge is located along a flat curve, the torsion caused by vehicle load also cannot be neglected. Because these phenomena could not easily be fully taken into consideration during the bridge design stage, it was therefore necessary to perform bridge monitoring in order to understand the bridge's mechanical characteristics. The details of the long-term monitoring system are depicted in Fig. 3.



Fig. 2 Long-span Bridge

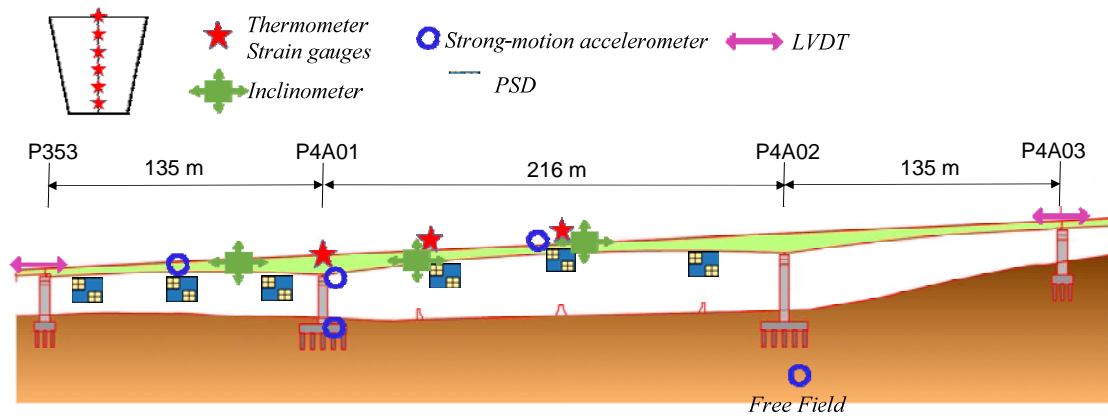


Fig. 3 The long-term monitoring system of the long-span Bridge

F-bent Double Decked Bridge

In order to avoid a geologically sensitive area on the east side, this elevated bridge carrying northbound lanes crosses Freeway No.1 and goes over to the southbound lane side, forming a co-constructed structure (with the northbound lanes on the upper level, and the southbound lanes on the lower level). The four-span continuous bridge has five piers numbered from P333 to P337, and each span has a length of 55 m (see Fig. 4). The two-level co-constructed design and high piers means that the bridge is strongly influenced by its own load, which has caused long-term eccentric effects. As a result, the bridge's lower structure tends to have local areas of large stress and overall displacement. In order to mitigate the bridge's structural weight, the upper and lower levels both employ a steel box girder bridge design, and the substructure consists of rectangular RC piers. In order to understand the effect of a long-term eccentric load and vibrations from earthquakes and traffic on this two-level bridge, monitoring of strain in the lower portions of the piers and the displacement of the cantilever cap beam in the lower load-bearing bridge were performed. The long-term monitoring system is shown in Fig. 5.



Fig. 4 F-bent Double Decked Bridge

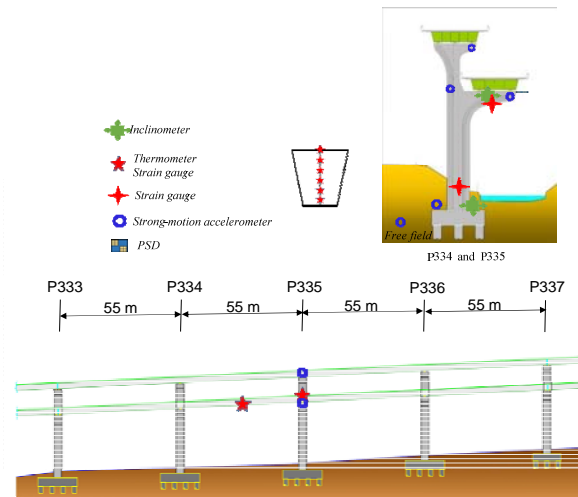


Fig. 5 The long-term monitoring system of the F-bent double decked bridge

#### Steel and Prestressed Concrete Composite Bridge

The upper structure of this steel and prestressed concrete composite bridge employs a uniform beam-depth design, and the eccentric piers have been designed to shorten the span (Fig. 6). Four piers numbered from P164 to P167 in this three-span continuous bridge (50 m, 85 m, and 50 m) were monitored. The steel beams are symmetrically arranged along the central part of the main span, and junctions between steel and concrete beams are located one-fourth of the way on the right and the left of the main span. Because of discontinuous stiffness where the two different materials are joined, there is a tendency for stress concentrations to occur at these points. The monitoring of this bridge can therefore shed light on the mechanical characteristics of these junctions between heterogeneous materials. The deployment of the long-term monitoring system is shown in Fig. 7.



Fig. 6 Steel and Prestressed Concrete Composite Bridge

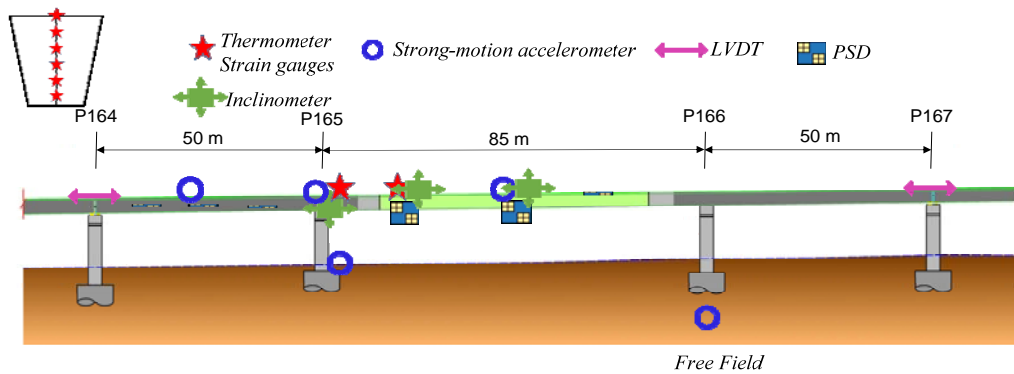


Fig. 7 The long-term monitoring system on the steel and prestressed concrete composite bridge

### 3. In-situ bridge experiments

Three types of in-situ experiments were conducted in order to obtain the engineering parameters of the bridges: a forced vibration experiment, static load experiment, and dynamic load experiment. An introduction to the features of each experiment is described below.

#### 3.1 Forced vibration experiment

A shaker using a set of symmetrical eccentric masses was employed in the forced vibration experiment as shown in Fig. 8; this device generated vibrations with a single frequency in a uniform direction, and the frequency could be adjusted from low to high (see Fig. 9). This allowed the resonance points at different locations and directions on the bridge to be found. The specifications of the forcing shaker are listed in Table 1. By changing the eccentric masses of the shaker, the applied external force, in the form of a simple harmonic wave, could be expressed as

$$p(t) = (m_e e \bar{\omega}^2) \sin(\bar{\omega}t) \tag{1}$$

Where  $m_e$  = mass of shaker,  $e$  = eccentricity,  $\bar{\omega}$  = excitation frequency

The foregoing equation can be used to obtain the simple harmonic response of a structure subject to forced vibrations

$$m\ddot{u} + c\dot{u} + ku = (m_e e \bar{\omega}^2) \sin(\bar{\omega}t) \tag{2}$$

Where  $m$  = mass of structures,  $c$  = damping coefficient,  $k$  = stiffness

Solving the second-order differential equation yields the following displacement vibration equation

$$u = \frac{m_e e \bar{\omega}^2}{k} R_d \sin(\bar{\omega}t - \varphi) \tag{3}$$

Where  $R_d = \frac{1}{\sqrt{(1-\beta^2)^2 + (2\xi\beta)^2}}$ ,  $\varphi = \tan^{-1} \frac{2\xi\beta}{1-\beta^2}$ ,  $\beta$  = frequency ratio,  $\xi$  = damping ratio

As shown in Eq. (3), apart from the effect of the structure's stiffness and damping ratio, a structure subject to forced vibration also reflects the eccentric masses of the forced shaker and the vibration frequency, and its characteristic parameters can be determined using a velocity meter or accelerometer. The eccentric masses and vibration frequency were taken as the experiment's control parameters.



Fig. 8 Forcing shaker



Fig. 9 Frequency of external force

Table 1 Specifications of the forcing shaker

Max. allowable rotation speed (Hz)	10
Max. eccentricity (N-m)	50.6
Max. output force (N)	44,440
Min. rotation speed required for max. output force (Hz)	4.6
Accuracy of rotation speed (Hz)	0.033
Weight (N)	7,377
Dimensions (m)	1×1.5×0.3

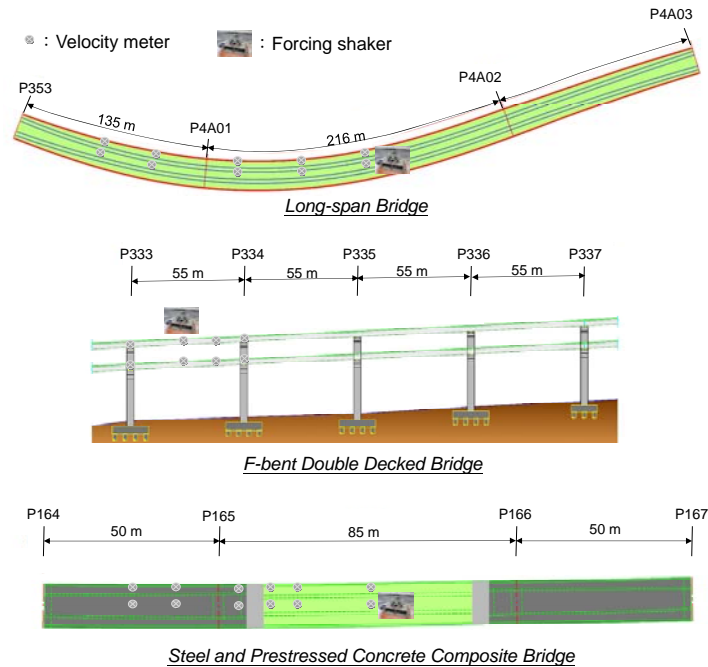


Fig. 10 Details of the forced vibration experiment

Forced vibration experiments were conducted on the three bridges described above. In the case of the long-span bridge, the shaker and 12 high-resolution velocity meters (longitudinal and transverse) were installed between piers P4A01 and P4A02, and eight velocity meters were installed between P353 and P4A01 on the side span. This provided a total of 20 velocity meters able to acquire vibration data. On the F-bent double decked bridge, the shaker was set up between P333 and P334 on the bridge's upper level, 12 high-resolution velocity meters (longitudinal, transverse, vertical) were installed on the upper and lower levels of the bridge between P333 and P334, and eight high-resolution velocity meters (longitudinal, transverse) were installed at the one-half and three-quarters points on the upper and lower levels from P333 to P334. A total of 20 velocity meters were thus installed on the bridge. In the case of the steel and prestressed concrete composite bridge, the forced shaker was set up between piers P165 and P166, and 24 high-resolution velocity meters were installed between piers P164 and P166 to acquire vibration data. The experimental sections, sensor locations, and the forcing shaker are shown in Fig. 10.

### 3.2 Static load experiment

The static load experiment was conducted using a level and laser rangefinder to conduct measurements. The precision of measurements using the level was 0.1 mm, and the precision of laser rangefinder measurements was 1 mm. The use of two measurement methods enabled the correctness of data to be checked. Level measurements were performed using points on near spans

as benchmarks, while laser measurements used the ground surface as a base line, and changes in observation points under the effect of loads was measured as shown in Fig. 11. However, as observation points under the large span bridge were located on a freeway, the laser rangefinder could not be used in this case. The corresponding displacement of observation points was measured for different load combinations ranging from 392.4 kN to 2354.4 kN (see Fig. 12).

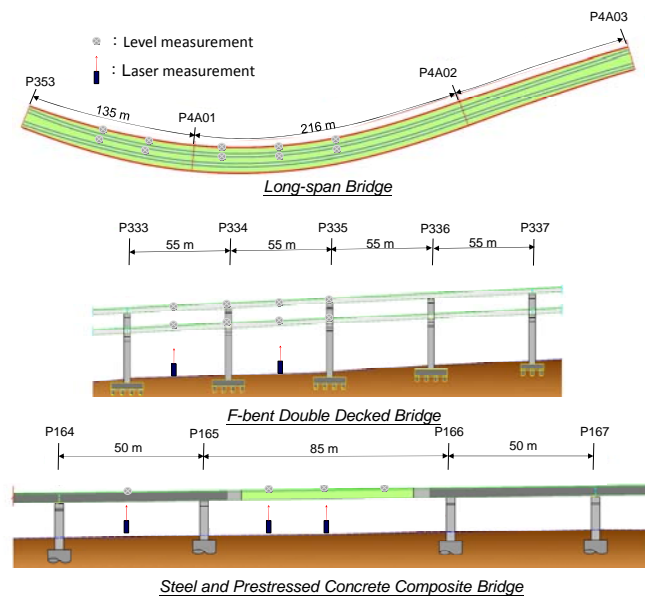


Fig. 11 Static load experiment

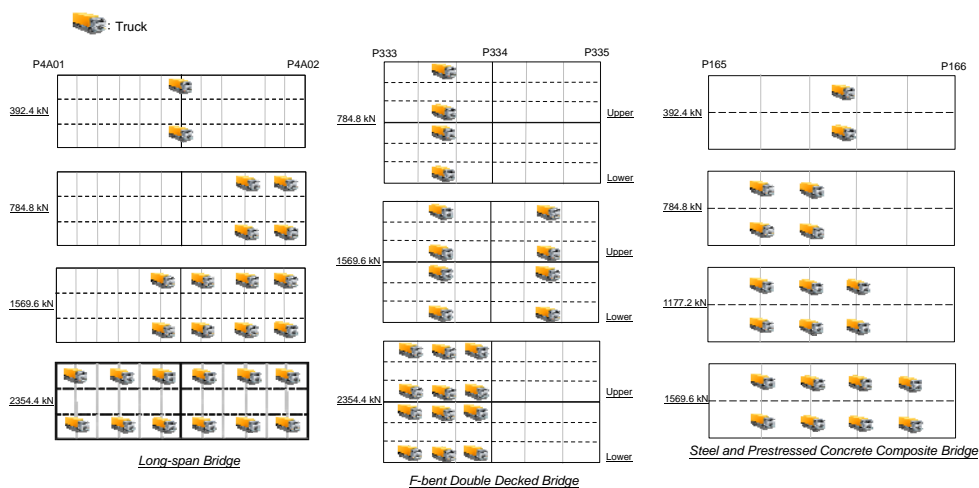


Fig. 12 Combinations employed in the static truck load experiment

### 3.3 Dynamic load experiment

The position sensitive device (PSD) method was used to determine the bridges' dynamic response. The dynamic load experiment employed two trucks weighing 196.2 kN each moving at speeds of 40 and 60 km/h from the adjacent span to the surfaces of the target spans. A fixed telescope mounted at a remote reference point was aimed at LEDs mounted under the box beams, and images of the LEDs were acquired by digital cameras shown in Fig. 13. Finally, image processing was employed to calculate the locations of the LEDs at different points in time. The signals captured by the cameras allowed changes in displacement to be obtained as the trucks passed through the vibrating unit of the bridge. The basic structure of this type of system is as shown in Fig. 14.

A PSD is a type of optical position sensor, and can measure the one-dimensional or two-dimensional location of a point above the sensing device. A PSD system as a whole comprises a video camera and monitoring targets. The video camera equipment used in this study consisted of ultra-high frequency and ultra-high resolution LED optical displacement gauge able to measure dynamic displacement with great precision. The LED optical displacement gauge possessed a maximum effective measurement distance of 300 m, and an ordinary nominal measurement distance of 100 m. When the measurement distance is only 100 m, the instrument had a field of view of 100 x 100 cm, and an excellent accuracy of 0.3 mm and high clarity could be provided when the measurement distance was 20 m. When the measurement distance was 200 m, the instrument could use a high-magnification lens offering a displacement resolution of 2 mm.

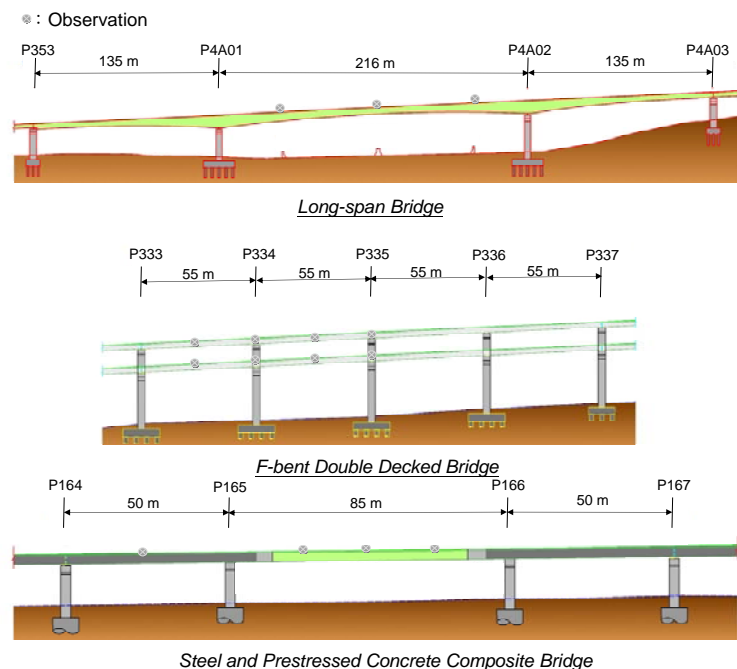


Fig. 13 Dynamic load experiment

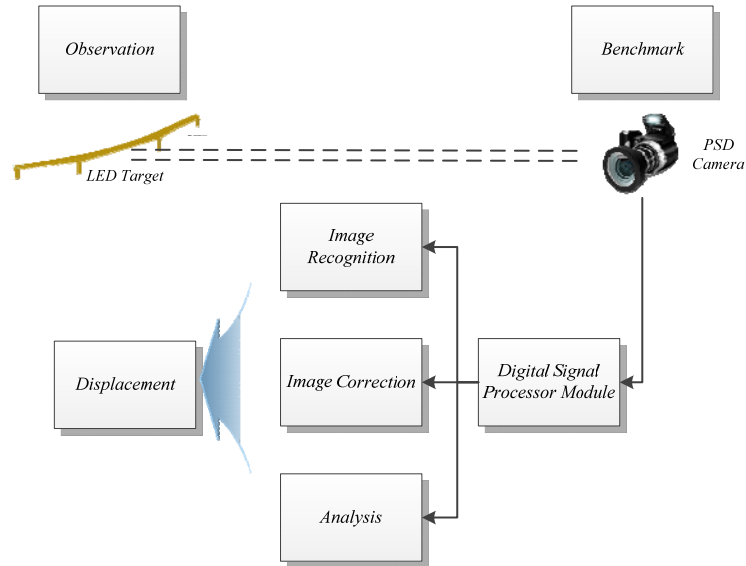


Fig. 14 PSD measurement system flowchart

#### 4. Verification of finite element bridge models and long-term monitoring results

In order to implement long-term monitoring systems, models for three special bridges were constructed based on the finite element method (FEM), which can be used to discretize an object as a set of basic finite elements connected to each other in a certain manner. Because the shapes of these basic elements can be different and combined in different ways, a structure can be modeled in a regular fashion, and the method can be used to effectively solve solid dynamics problems involving complex geometric shapes or boundary conditions.

With regard to cutting of the finite elements, the physical elements were cut into small zones with different sizes and types. Because of tiny size, each small element was assumed to have identical internal characteristics. Differences in characteristics between different elements allowed the simplification of complex problems in analysis. It should be noted that the more finely a grid were divided, the more precise the values that could be obtained. This approach is close to that of a real model, but as the grid size changes, the amount of computing time needed also varied. As a result, the selection of an appropriate grid size and judgment of convergence of elements had to be carefully considered to enhance analytical efficiency and correctness.

As the chosen elements had to reflect the physical characteristics of the structure to be analyzed, point elements, beam elements, area elements, and solid elements were included. After selecting appropriate types of elements, the element material parameters were input, and the material parameters were adjusted slightly for the different types of elements. Based on the original blueprints, the stiffeners of the box girder and the steel tendons of the prestressed concrete were considered carefully. The individual models used in this study all employed two or more types of elements in analysis. Solid elements were employed for the prestressed concrete and bridge piers,

area elements were employed for steel plate, and beam elements were used for prestressed steel tendons. The proposed procedures enabled the modeling of each bridge to reflect its practical engineering characteristics.

In this study, as the load of the trucks on the bridge caused vibration and strain, it was necessary to divide large beam elements finely in order to obtain relatively accurate dynamic response when analyzing strain. As can be seen from Table 2, the elements used were finely-divided and large in quantity in order to precisely model a bridge as a whole. The material parameters of prestressed concrete consisted of a compressive strength  $f_c = 3433.5 \text{ N/cm}^2$  and a unit weight of  $23.57 \text{ kN/m}^3$ ; the material parameters of steel plate consisted of a Young's modulus of  $E=200 \text{ GPa}$  and a unit weight  $77 \text{ kN/m}^3$ ; and the material parameter of prestressed steel tendons consisted of a Young's modulus  $E=189 \text{ GPa}$ . All the parameters were obtained through a series of material tests. In addition, non-structural components, including pipelines, side balusters, and bolts, were also included in the total mass of the superstructure.

Long-term monitoring of the three special bridges began in October 2013. In order to demonstrate the reliability and stability of the instrumentation, data recorded at specific locations on the long-span bridge is presented here. With the support of the fine-tuned finite element models and the continuous database resulting from long-term monitoring, alarm thresholds can be determined as a reference for bridge managers when performing rapid diagnosis and evaluation in the near future.

Table 2 Finite element types and quantities

Element Type	Long-span Bridge	F-bent Double Decked	Steel and Prestressed
		Bridge	Concrete Composite Bridge
Solid	96,161	285,449	255,246
Plate	208,651	72,712	18,440
Beam	-	4,150	4,400

#### 4.1 Comparison of fundamental frequency in forced vibration experiments

Velocity meters were employed in the forced vibration experiment to measure speed response with a sampling frequency of 200 Hz, and the fast Fourier transform was then used to transform the time domain to the frequency domain and obtain the fundamental frequency. The finite element method was used to perform characteristic analysis for three special bridges, and the results were compared with those of the forced vibration experiment, as shown in Table 3. The results indicate that the first mode could be precisely expressed for the three bridges, and although the second mode had some minor error, it was also acceptable. It can be seen from Eq. (3) that the amplitudes obtained in the forced vibration experiment were proportional to  $\bar{\omega}^3$ , and changes in the applied frequency affected the amplitude. As a consequence, it was necessary to normalize the measured amplitudes, which were uniformly divided by  $\bar{\omega}^3$  to obtain the natural vibration frequencies from the frequency spectra. The values for the long-span bridge before and after normalization are shown in Fig. 15. When the applied frequency was increased, the amplitude increased with

frequency before normalization. This phenomenon does not result from the applied frequency being close to a bridge's natural frequency, and may cause mistaken determination of the bridge's natural vibration frequency. A bridge's natural vibration frequency can therefore best be determined after normalization.

Table 3 Comparison of fundamental frequencies

Mode(Hz)	Long-span bridge		F-bent double decked bridge		Steel and prestressed concrete composite bridge	
	Experiment	Analysis	Experiment	Analysis	Experiment	Analysis
1	0.8972	0.8972	0.7996	0.8053	0.8911	0.8915
2	1.3	1.316	1.204	1.077	1.0986	1.0858

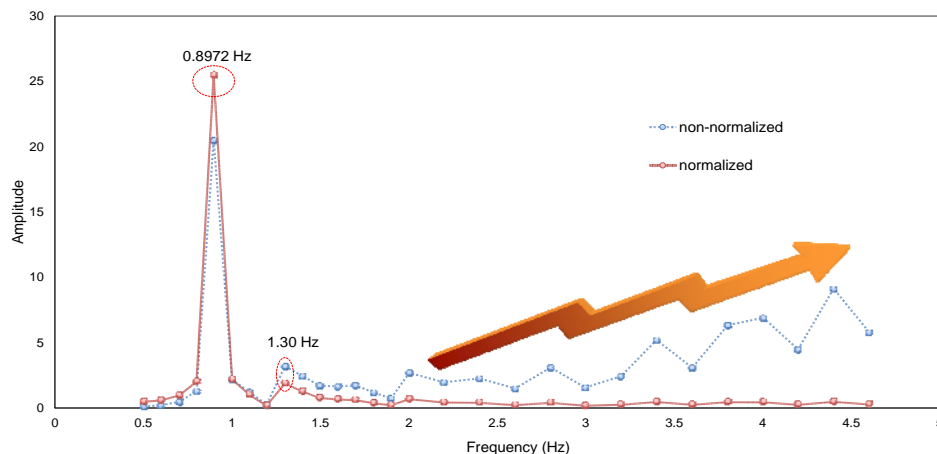


Fig. 15 Comparison of normalized and non-normalized frequency spectra for the long-span bridge

#### 4.2 Comparison of static vehicle load results

The static load experiment involved loads varying from 392.4 kN to 2354.4 kN. When testing the effect of vehicle load on the long-span bridge, the observation point was located half-way along the main span, which extended for 216 m between piers P4A01 and P4A02 in Fig. 16. Loads were applied to the 110 m span between P333 and P335 on the F-bent double decked bridge, and the observation point was located on the lower level half-way between P333 and P334 as depicted in Fig. 17. Loads were applied to the 85 m span between P165 and P166 on the steel and prestressed concrete composite bridge, and the observation point was located half-way along the main span as shown in Fig. 18.

A comparison of the results of static load experiments for the three special bridges is shown in Table 4. As the long-span bridge crossed a freeway, the laser rangefinder could not be used. The

results indicate that stiffness can be effectively expressed by the finite element models of the three bridges, and the displacement of the observation points can be seen when a 392.4-kN load was applied to the long-span and steel and prestressed concrete beam bridges, and when an 784.8 kN load was applied to the F-bent double decked bridge (392.4 kN each on the upper and lower levels). This information can be used to confirm the reasonableness of measurements in the dynamic experiment.

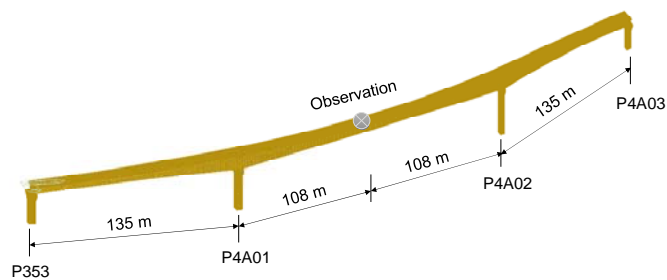


Fig. 16 Finite element model and observation points for long-span bridge

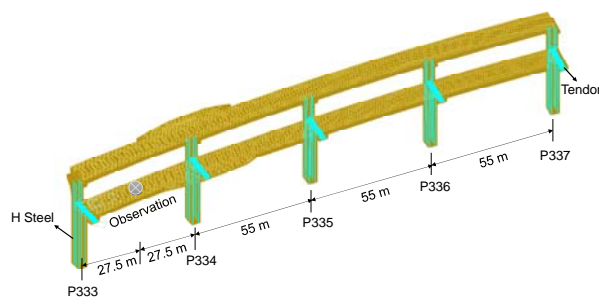


Fig. 17 Finite element model and observation points for F-bent double decked bridge

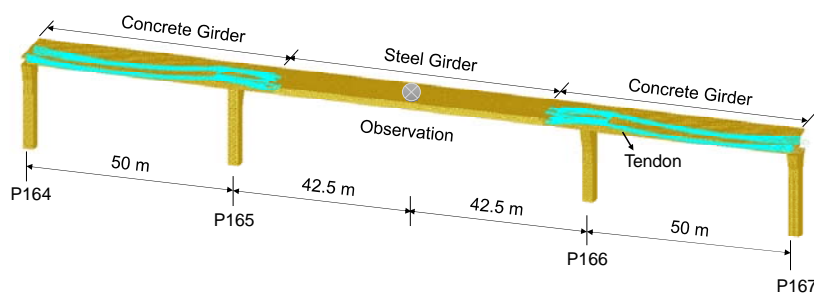


Fig. 18 Finite element model and observation points for steel and prestressed concrete composite bridge

Table 4 Comparison of results of static load experiment and analysis

	Long-span bridge				F-bent double decked bridge			Steel and prestressed concrete composite bridge			
Load (kN)	392.4	784.8	1569.6	2354.4	784.8	1569.6	2354.4	392.4	784.8	1177.2	1569.6
Level (cm)	-1.87	-1.99	-5.17	-6.09	-0.45	-0.44	-0.85	-0.65	-1.03	-1.38	-1.59
Laser (cm)	-	-	-	-	-0.4	-0.2	-0.6	-0.6	-0.9	-1.5	-1.7
Analysis (cm)	-1.87	-1.24	-4.79	-6.21	-0.47	-0.35	-1.09	-0.63	-0.81	-1.37	-1.61

#### 4.3 Comparison of dynamic vehicle load results

After correcting the natural frequency and stiffness in the finite element model on the basis of the results of the forced vibration and static load experiments, the dynamic load experiment was employed to verify the bridges' dynamic behavior. The traveling loads on the bridges' superstructures in the bridge models was consistent with the experimental trucks driven on the three bridges at speeds of 40 km/h and 60 km/h, and the trucks were considered to be impulsive loads passing across the bridges. The impulsive loads acted instantaneously and then vanished, and the time differences were determined by the vehicle speed and the distance between the nodes in the constructed model. A preliminary study considering the load-bridge interaction for dynamic load testing was conducted and compared with the original numerical model. The results showed that almost no difference was observed between the two systems, as the mass of the dynamic load was relatively small compared with the mass of the bridge structure, which implied that the load-bridge interaction effect could be neglected.

The performance of the proposed PSD system was examined on the basis of the numerical simulation results. The widely-used fast Fourier transform method was applied to evaluate the distribution of the energy in the frequency domain, and the high-frequency signal was then removed from the field experiment data. To extract bridge characteristics from the influence of ambient noise, noise in real-time displacement monitoring data from the PSD system was filtered through a low-pass threshold filter at 7.5 Hz, which reflected the research conducted by Sung *et al.* (2012), and data collected from the superstructure and the substructure were used to determine the differences between theoretical and measured data.

Figs. 19-24 display comparisons of the dynamic displacement of observation points on the three bridges, and the locations of the observation points are as shown in Figs. 16-18. As shown in the figures, in all three cases, the initial displacements measured by PSDs were not zero, which was because the truck had started to accelerate from the adjacent span to the observation point. In the case of the long-span bridge, the dynamic behavior can be accurately expressed by the finite element model, and the dynamic response trends fit the experimental results quite closely.

Furthermore, when trucks passed the vibrating elements of the long-span bridge, the results of free vibration analysis also conformed closely to the results of experiment. When the dynamic load experiment was performed on the F-bent double decked bridge, the experimental dynamic waveform trends were compatible with those of the simulation, except for slight differences caused by unstable truck speed after 10 seconds. While the steel and prestressed concrete beam bridge experiment also yielded similar results, with regard to the stiffness characteristics of the prestressed concrete beam section, the long measurement distance resulted in a high level of noise after the trucks had passed, which could not be reflected in the model.

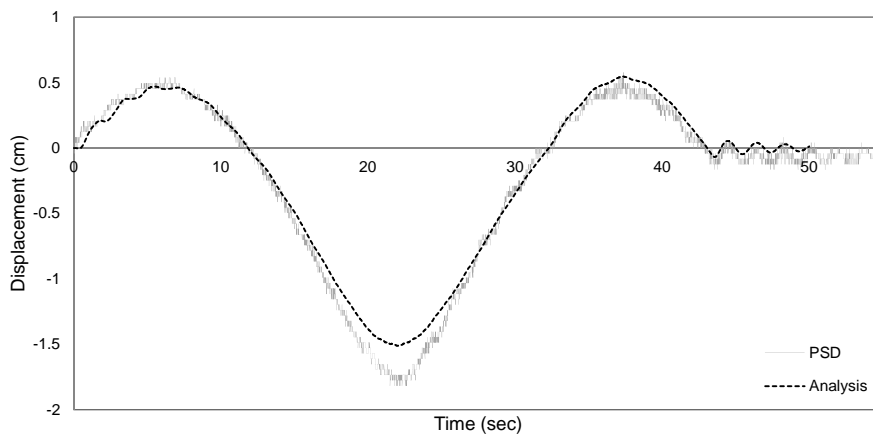


Fig. 19 Long-span bridge - comparison of observation point with vehicle speed of 40 km/h

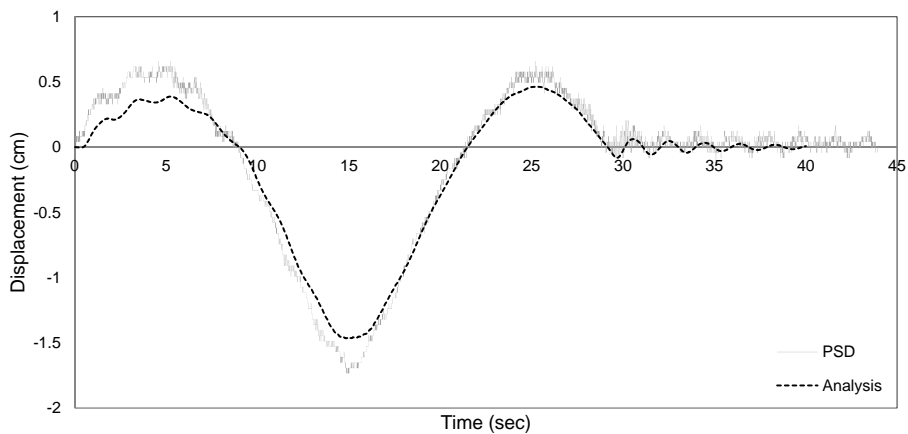


Fig. 20 Long-span bridge - comparison of observation point with vehicle speed of 60 km/h

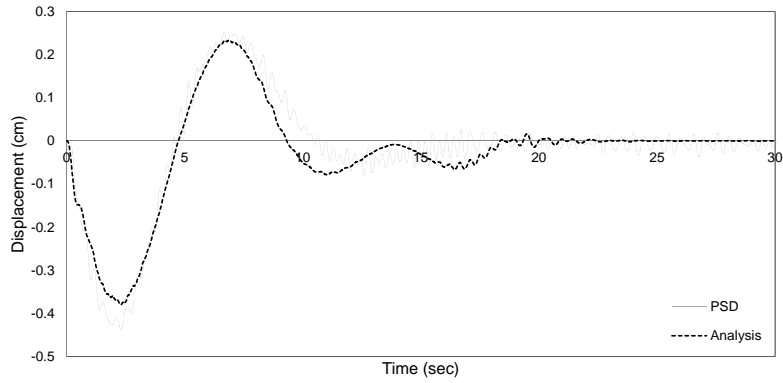


Fig. 21 F-bent double decked bridge - comparison of observation point with vehicle speed of 40 km/h

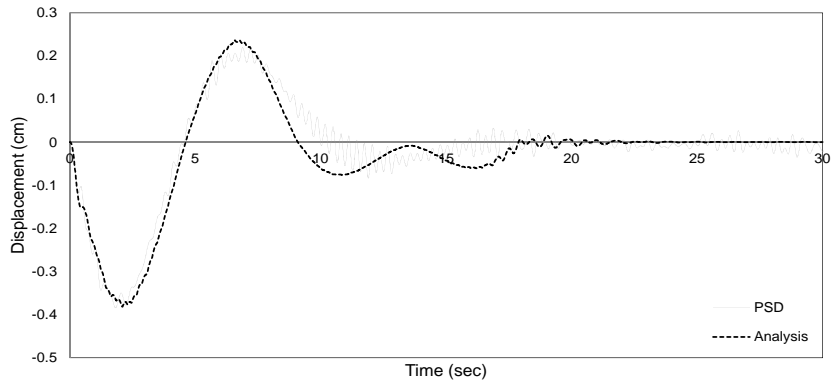


Fig. 22 F-bent double decked bridge - comparison of observation point with vehicle speed of 60 km/h

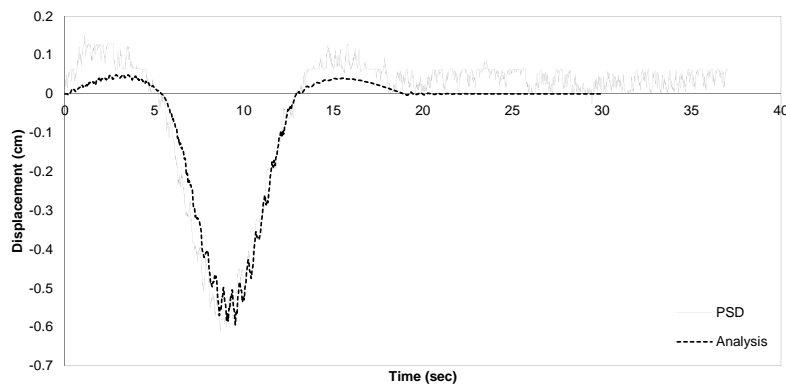


Fig. 23 Steel and prestressed concrete composite bridge - comparison of the observation point with vehicle speed of 40 km/h

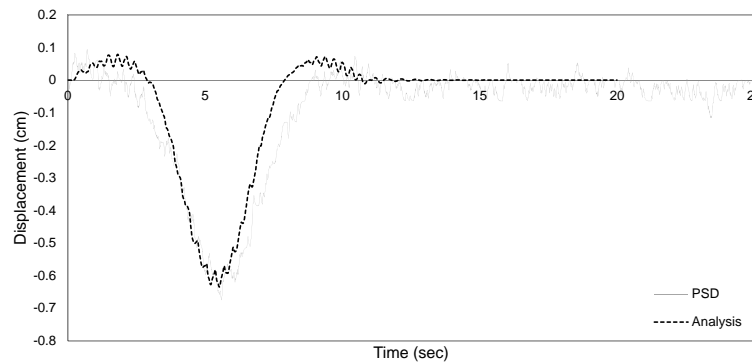


Fig. 24 Steel and prestressed concrete composite bridge - comparison of the observation point with vehicle speed of 60 km/h

#### 4.4 Long-term monitoring results

The long-term monitoring systems began operation on all three bridges in the middle of October 2013, following correction of the finite element model through in-situ experiments. The monitoring data collected on the long-span bridge between October 7, 2013 and February 3, 2014 is shown in Figs. 25-27, and reflects a constant sampling interval of 10 minutes. As noted, the instrumentation had been working normally, and all of the measured data was found to be in a reasonable range following expected trends. In order to monitor the distribution of the temperature gradient of the mid-span between P4A01 and P4A02, six thermometers numbered Thermometer01 – Thermometer06 were installed along the height of the box girder (see Fig. 25). Apart from daily temperature changes, in which the average temperature gradually varied between 25°C and 15°C, the large height of the beams was reflected in the temperature gradient. The temperature difference in the direction of the beam height could be additionally considered in the numerical model to improve the precision of structural health monitoring. Accompanying with the thermometers, six strain gauges numbered Strain gauge01-Strain gauge06 were also attached to the surface of the box girder (see Fig. 26). The signal from Strain gauge02 was found to have significant error, and was ignored in our analysis. As shown in the figure, the observed compression and tension in the top and bottom flanges was found to be in the elastic range, which preliminarily supports the safety of the bridge. Furthermore, although the signal from strain gauge S02 was lost during the installation process, the stress condition was determined via data from the remaining strain gauges, which were distributed in the mid-span section between P4A01 and P4A02 of the long-span bridge. The displacement measured by the LVDT of pier P4A03 varied from -0.4 mm to +1.4 mm, which also followed the expected physical trend (see Fig. 27). In general, the bridges have been reliably monitored by the structural health monitoring systems. Since earthquakes occur frequently in Taiwan, strong ground motion events recorded by the accelerometers can provide additional data for system identification. Moreover, the database containing data from the static data logger can be used to support the determination of the alarm threshold and the refinement of the established finite element model. Through the integration of the finite element model and long-term monitoring data, rapid diagnosis and evaluation can be conducted by bridge managers when abnormalities are observed during the continuous monitoring process.

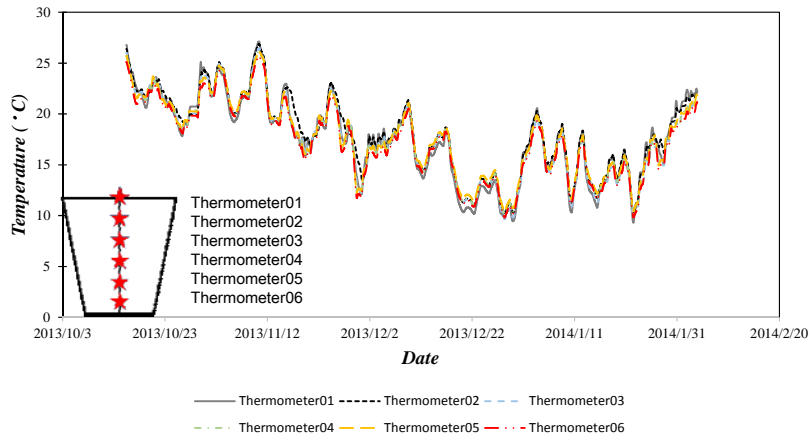


Fig. 25 Temperature gradient measured on the mid-span section between P4A01 and P4A02 of the long-span bridge

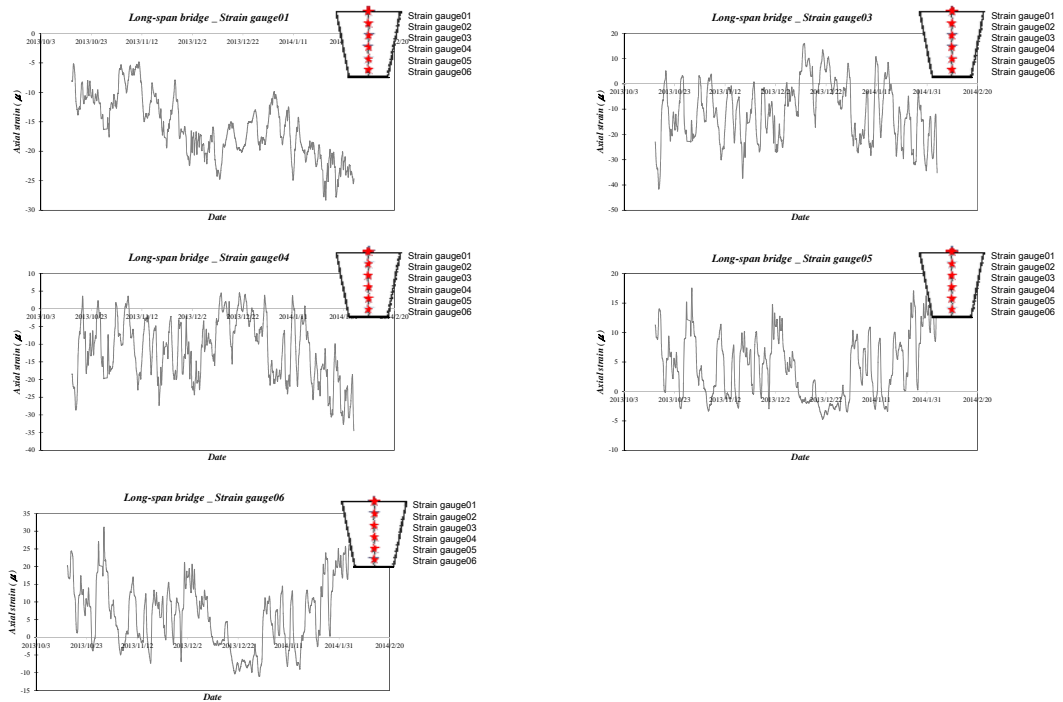


Fig. 26 Strain measured on the mid-span section between P4A01 and P4A02 of the long-span bridge

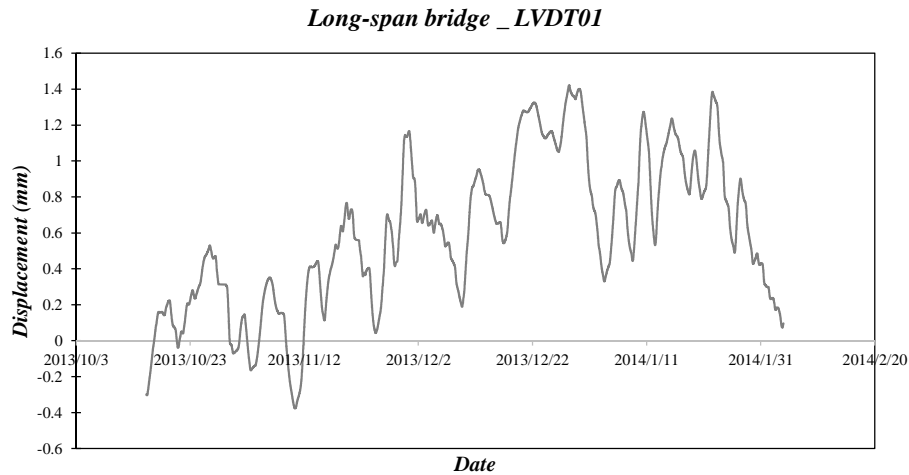


Fig. 27 Displacement measured from the LVDT of pier P4A03 on the long-span bridge

## 5. Conclusions

This study performed monitoring of three special bridges along an extended section of the freeway system in Taiwan, including the deployment of long-term monitoring systems, the implementation of in-situ experiments, and the establishment of finite element models used to construct three-dimensional physical models for use in long-term monitoring systems. The following conclusions were reached after analysis and comparison:

1. Different types of sensor were deployed in in-situ bridge experiments and long-term bridge monitoring system in order to understand the short-term and long-term behavior of the monitored bridges. The mechanical characteristic of static, dynamic and long-term loads, including those caused by temperature changes and earthquakes, could be determined through the specific arrangement.
2. Through the support of the developed finite element model, it was found that a limited number of sensors could be used to monitor the real-time condition of the three bridges with only a limited maintenance budget. Based on the monitoring results, additional sensors could be further considered on sections possibly suffering damage in order to strengthen the performance of the system in the future.
3. The natural frequencies determined from the finite element models were compared with the data obtained from in-situ forced vibration experiments. The similar results demonstrated that the natural frequencies of the three bridges could be determined using the finite element models. With this support, assessment of the three bridges can be performed rapidly in the future.
4. A series of static load test revealed that the actual stiffness of the bridges was successfully reflected in numerical simulation conducted using bridge models based on loading patterns.
5. Following the examination of natural frequency and bridge stiffness, simulation of dynamic load testing results yielded satisfactory estimates of peak response and trends,

- demonstrating the feasibility and reliability of applying the established models in long-term monitoring.
6. The high-resolution advanced PSD system employed in the mobile load experiments can directly provide high-precision real-time structural displacement data, and can largely eliminate the problem of insufficient precision of conventional displacement measurement methods.
  7. The integration of in-situ load experiments and numerical modeling enhanced the feasibility of long-term bridge monitoring systems. No damage has been detected by monitoring systems thus far, and the recorded data will be used to update the model to improve its reliability.
  8. Since the instrumentation system currently comprises traditional wired sensors and MEM-based sensors, advanced technology may be considered to increase the integrity of the system.
  9. A combination of in-situ experiments, which provide the bridges' initial conditions, and numerical models can facilitate bridge safety evaluation and life-cycle management via use of the proposed bridge monitoring system.
  10. As the bridges are newly-constructed, the critical threshold to detect damage or deterioration will be determined using the updated numerical model and long-term databases.

## References

- Chan, T.H.T., Yu, L., Tam, H.Y., Ni, Y.Q., Liu, S.Y., Chung, W.H. and Cheng L.K. (2006), "Fiber Bragg grating sensors for structural health monitoring of Tsing Ma bridge: Background and experimental observation", *Eng. Struct.*, **28**(5), 648-659.
- Costa, B.J.A. and Figueiras, J.A. (2012), "Evaluation of a strain monitoring system for existing steel railway bridges", *J. Constr. Steel Res.*, **72**, 179-191.
- Cury, A., Cremona, C. and Dumoulin, J. (2012), "Long-term monitoring of a PSC box girder bridge: Operational modal analysis, data normalization and structural modification", *Mech. Syst. Signal Pr.*, **33**, 13-37.
- Gomez, H.C., Fanning, P.J., Feng, M.Q. and Lee, S. (2011), "Testing and long-term monitoring of a curved concrete box girder bridge", *Eng. Struct.*, **33**(10), 2861-2869.
- Kim, N.S. and Cho, N.S. (2004), "Estimating deflection of a simple beam model using fiber optic Bragg-grating sensors", *Exper. Mech.*, **44**(4), 433-439.
- Lee, J.J. and Shinozuka, M. (2006), "Real-time displacement measurement of a flexible bridge using digital image processing techniques", *Soc. Exper. Mech.*, **46**(1), 105-114.
- Li, D., Zhou, Z. and Ou, J. (2012), "Dynamic behavior monitoring and damage evaluation for arch bridge suspender using GFRP optical fiber Bragg grating sensors", *Opt. Laser Technol.*, **44**(4), 1031-1038.
- Lnaudi, D., Vurpillot, S., Glisic, B., Kronenberg, P. and Lloret, S. (1999), "Long-term monitoring of a concrete bridge with 100+ fiber optic long-gage sensors", *Proceedings of the SPIE's International Symposium on Nondestructive Evaluation Techniques for Aging Infrastructure & Manufacturing*.
- Lnaudi, D. and Vurpillot, S. (1999), "Monitoring of concrete bridges with long-gage fiber optic sensors", *J. Intel.Mat. Syst. Str.*, **10**, 280-292.
- Nassif, H.H., Gindy, M. and Davis, J. (2005), "Comparison of laser Doppler vibrometer with contact sensors for monitoring bridge deflection and vibration", *NDT& E Int.*, **38**(3), 213-218.
- Olaszek, P. (1999), "Investigation of the dynamic characteristic of bridge structures using a computer vision method," *Measurement*, **25**(3), 227-236.

- Patjawit, A. and Kanok-Nukulchai, W. (2005), "Health monitoring of highway bridges based on a global flexibility index", *Eng. Struct.*, **27**(9), 1385-1391.
- Ribeiro, D., Calçada, R., Delgado, R., Brehm, M. and Zabel, V. (2012), "Finite element model updating of a bowstring-arch railway bridge based on experimental modal parameters", *Eng. Struct.*, **40**, 413-435.
- Stephen, G.A., Brownjohn, J.M.W. and Taylor, C.A. (1993), "Visual monitoring of the Humber Bridge", *Eng. Struct.*, **15**(3), 197-208.
- Sung, Y.C., Miyasaka, T., Lin, T.K., Wang, C.Y. and Wang, C.Y. (2012), "A case study on bridge health monitoring using position sensitive detector technology," *Struct. Control Health Monit.*, **19**(2), 295-308.
- Wahbeh, A.M., Caffrey, J.P. and Masri, S.F. (2003), "A vision-based approach for the direct measurement of displacements in vibrating systems", *Smart Mater. Struct.*, **12**(5), 785-794.